

NJC

Accepted Manuscript



This is an *Accepted Manuscript*, which has been through the Royal Society of Chemistry peer review process and has been accepted for publication.

Accepted Manuscripts are published online shortly after acceptance, before technical editing, formatting and proof reading. Using this free service, authors can make their results available to the community, in citable form, before we publish the edited article. We will replace this *Accepted Manuscript* with the edited and formatted *Advance Article* as soon as it is available.

You can find more information about *Accepted Manuscripts* in the [Information for Authors](#).

Please note that technical editing may introduce minor changes to the text and/or graphics, which may alter content. The journal's standard [Terms & Conditions](#) and the [Ethical guidelines](#) still apply. In no event shall the Royal Society of Chemistry be held responsible for any errors or omissions in this *Accepted Manuscript* or any consequences arising from the use of any information it contains.

**FTIR, Magnetic and Mössbauer Investigations of Nano-crystalline $\text{Fe}_x\text{Co}_{1-x}$
($0.4 \leq x \leq 0.8$) Alloys Synthesized via Superhydride Reduction Route**

Shankar B. Dalavi,^a M. Manivel Raja^b and Rabi N. Panda^{a*}

^a*Department of Chemistry, BITS-Pilani, K. K. Birla Goa Campus, Zuarinagar, Goa-403726, India.*

^b*Defence Metallurgical Research Laboratory, Hyderabad-500058, India.*

*Corresponding author. Tel.: 0091-08322580311, Fax: 0091-08322580280.

Email address: rnp@goa.bits-pilani.ac.in

Abstract:

The present investigation reveals the synthesis of capped nano-crystalline $\text{Fe}_x\text{Co}_{1-x}$ ($0.2 \leq x \leq 0.8$) alloys via superhydride reduction route using oleic acid and oleylamine as stabilizing agents. The synthesized nano-particles are stable against oxidation in air atmosphere (air stable) at room temperature (298K). Structure-properties correlation in FeCo alloys have been attempted using Fourier transform infrared spectroscopy (FTIR), X-ray diffraction (XRD), transmission electron microscopy (TEM), magnetic and Mössbauer measurements. FTIR study indicates the presence of organic content at the surface of the nanoparticles which helps in the stabilization of the FeCo samples in air atmosphere. FeCo alloys crystallize in pure α -phase with the increase in the values of lattice parameters with the increase in Fe content, i.e. $2.836(\pm 4) \text{ \AA}$, $2.852(\pm 2) \text{ \AA}$, $2.859(\pm 1) \text{ \AA}$ and $2.868(\pm 1) \text{ \AA}$ for $x = 0.2, 0.4, 0.6$ and 0.8 , respectively. Average crystallite sizes and TEM particle sizes were found to be in the range of $\approx 23\text{-}38 \text{ nm}$ and $11\text{-}51 \text{ nm}$, respectively. The values of the saturation magnetization (M_s) for FeCo alloys range from $71.1\text{-}92.5 \text{ emu/g}$ for heat treated materials and $93.1\text{-}142.2 \text{ emu/g}$ after corrections for organic wt % at the surface of the materials. The observed values of effective anisotropy constants (K_{eff}) of $\text{Fe}_x\text{Co}_{1-x}$ alloys from field cooled (FC) and zero field cooled (ZFC) studies (i.e. 1.5 kJ/m^3 , 4.6 kJ/m^3 and 14.3 kJ/m^3 for $x = 0.4, 0.6$ and 0.8 , respectively) reveal the contribution from the reduced particle size and surface anisotropy. The maximum value of hyperfine field for $\text{Fe}_x\text{Co}_{1-x}$ alloys was found to be 34.9 T for $\text{Fe}_{0.6}\text{Co}_{0.4}$ composition and has been interpreted on the basis of enhancement of Fe moments in the disordered crystal lattice.

Keywords: Chemical synthesis, X-ray diffraction, Nanocrystalline materials, Magnetic materials.

1 Introduction

Recently, research on FeCo alloys have received increasing attention of scientists because of their technological properties; such as large permeability, high saturation magnetization and Curie temperature.^{1,2} These technological properties depend on particle size, shape, surface morphologies, crystal anisotropies and inter-particle interactions. In nanometer scale, FeCo alloys are important for their applications as building units for functional nanomaterials,³ magnetic resonance imaging,⁴ magnetic recording,⁵ biomedical applications⁶ and microwave absorbing materials.⁷ The development of metal and alloys nanoparticles with high permeability for high temperature applications has become a subject of intensive research and cannot be achieved by the existing soft magnetic materials; for example: ferrites.⁸ However, the issues need to be addressed is how to improve material stability and surface protection around FeCo nanomaterials. Therefore, synthesis, characterization and magnetic properties of FeCo nanomaterials are important topics for investigation.

Various synthetic techniques have been used in the literature for the synthesis of FeCo alloys; such as: thermal decomposition,⁹ chemical reduction process,¹⁰ chemical vapor deposition,¹¹ polyol process,¹² sol gel process¹³ etc. Amongst all these methods employed, chemical reduction process is very convenient in order to prepare nano-meter size particles of transition metal/alloys with controlled size and shape morphologies. The resulting controlled size and shape may be expected to arise from the flexibility of using different concentrations of metal ions in organic solvents along with the capping agents. Such an approach has already been established in the literature for the synthesis of FePt nanoparticles.¹⁴ Various reducing agents, such as: sodium borohydride, superhydride, hydrazine etc., can be used for the preparation of FeCo alloy nanoparticles of different sizes.¹⁵ In superhydride route, metal ions can be reduced in the presence of organic solvents in order to produce nanomaterials with relatively smaller size range (< 10 nm) which may be suitable for applications in magnetic recording media. However, scanty literatures are available on the preparation of FeCo alloys by superhydride route. Preparation of air stable nanocrystalline FeCo alloys of different compositions with controlled shape and size by using superhydride as a reducing agent in organic medium has not been reported till-to-date. In this study, we have prepared air stable $\text{Fe}_x\text{Co}_{1-x}$ ($0.2 \leq x \leq 0.8$) alloy

nanoparticles of various compositions by superhydride method. The nanomaterials were characterized using FTIR, XRD, TEM and magnetic measurements. The magnetic properties are investigated in detail using superconducting quantum interference device (SQUID) magnetometer and Mössbauer study. Finally, we have attempted structure-properties correlation in the synthesized FeCo nanomaterials.

2 Experimental

For the present investigation, we have procured ferric chloride ($\text{FeCl}_3 \cdot 6\text{H}_2\text{O}$), cobalt chloride ($\text{CoCl}_2 \cdot 6\text{H}_2\text{O}$) from Molychem, India and oleic acid, oleylamine, diphenyl ether, superhydride (LiBEt_3H , 1 M in THF) from Sigma Aldrich, USA. These chemicals were used without further purification for the synthesis.

2.1 Synthesis of FeCo alloy nanoparticles:

The synthetic procedure adopted is quite similar to that of reported by Shen et al. for the preparation of CoPt materials.¹⁶ In summary, for the synthesis of $\text{Fe}_x\text{Co}_{1-x}$ alloys ($x = 0.2, 0.4, 0.6, 0.8$), 1 mmol of stoichiometric amount of metal chlorides were mixed with 25 ml diphenyl ether in the 250 ml three neck flask and stirred under high purity N_2 (g) atmosphere for 2 h duration at room temperature. The mixture was heated to 100 °C for the time duration of 20 min. 0.32 ml oleic acid (1 mmol) and 0.34 ml oleylamine (1 mmol) were added to dissolve the metal precursors. Next, the solution was heated to 200 °C for the time duration of 10 min and 3 ml superhydride solution (LiBEt_3H , 1 M in THF) was added drop by drop into the hot solution over a period of 5 min. At this stage, black solids were precipitated out in the solution. The black solution was stirred at 200 °C for 1 h under N_2 (g) atmosphere in order to remove lower boiling solvents. The mixture was cooled down to room temperature and added 15 ml ethanol along with 0.16 ml oleic acid and 0.17 ml oleylamine. The black solids were separated by centrifugation at 4500 rpm for 5 min, decanted out upper clear liquid. Black solids were again dispersed in 10 ml ethanol containing 0.16 ml oleic acid and 0.17 ml oleylamine. The reaction mixture was centrifuged in order to separate the resulting solid (i.e. as-prepared materials). Finally, the as-prepared FeCo alloy samples were heat treated in high purity N_2 (g) atmosphere at 600 °C for 2 h and used for further studies.

2.2 Characterization:

FeCo alloys with different compositions were characterized by FTIR, C-H-N-S analysis, XRD, TEM, Mössbauer spectroscopy and magnetic measurements. FTIR spectra were recorded using FTIR spectrophotometer (Model: SHIMADZU, IRAffinity-1). CHN content in the nanomaterials was measured using elemental analyzer (Model: Vario Micro cube). The XRD patterns were recorded using a powder X-ray diffractometer (Model: Mini Flex II, Japan) using Cu K α radiation, ($\lambda = 0.15405$ nm) at the scan speed of 3° per minute. The phase purity was ascertained using X-ray diffraction. Crystallite size was estimated using Scherrer equation, $t = 0.9\lambda/B\cos\theta$, where t is crystallite size, λ is wavelength of the X-ray radiation, B is FWHM in radian and θ is the diffraction angle.¹⁷ The size, shape and selected area electron diffraction (SAED) of the products were examined by TEM (Model: PHILIPS CM200). The average diameters of various particles have been plotted against their frequency of occurrence and the mean positions were noted as TEM particle sizes. Spacing between the crystal planes (d -values) were calculated by taking reciprocal of the distance of the observed diffraction spots from the centre and indexed accordingly. Magnetization versus field (M vs H) at room temperature as well as FC and ZFC magnetization measurements at low temperatures (5-300 K) were carried out on solid powder materials of Fe $_x$ Co $_{1-x}$ alloys ($x = 0.4, 0.6, 0.8$) using SQUID magnetometer (Model: M/S Quantum Design USA). The sample was first cooled to 5 K in the absence of external magnetic field and then warmed to 300 K in the presence of external magnetic field and the magnetization is recorded as ZFC. The FC measurements were done after ZFC measurements and the magnetization is recorded while cooling the sample down from 300 to 5 K with 100 Oe field. The Mössbauer spectra of Fe $_x$ Co $_{1-x}$ alloys ($x = 0.4, 0.6, 0.8$) were recorded at room temperature using a constant acceleration spectrometer (Model: M/s. FastCom Tech, Germany) with 25 mCi ^{57}Co (Rh) gamma ray source. The experimental spectrum was analyzed using PCMO5 II least-squares fitting program. The values of the isomer shifts were reported with respect to natural iron(Fe) foil.

3 Results and Discussion

$\text{Fe}_x\text{Co}_{1-x}$ alloys ($x = 0.2, 0.4, 0.6, 0.8$) nano-particles synthesized by superhydride route were annealed at 600°C and subjected to further investigations.

3.1 Investigation of nature of organic capping layer:

In order to ascertain the chemical nature of the capping layer, we have performed organic content analysis by CHN and FTIR on the samples, heat treated at 600°C under nitrogen gas atmosphere. The CHN contents were found to be 34.9, 32.7 and 23.4 wt% for $\text{Fe}_{0.4}\text{Co}_{0.6}$, $\text{Fe}_{0.6}\text{Co}_{0.4}$ and $\text{Fe}_{0.8}\text{Co}_{0.2}$ alloy compositions, respectively. The major fraction of materials in the organic capping layer were carbon, i.e. 33.4, 31.1 and 21.4 with C:H ratios 20.8:1, 19.8:1 and 10.7:1 for $\text{Fe}_{0.4}\text{Co}_{0.6}$, $\text{Fe}_{0.6}\text{Co}_{0.4}$ and $\text{Fe}_{0.8}\text{Co}_{0.2}$, respectively. To be noted that C:H ratio used during the synthesis was 6:1. The observation of higher C:H ratios in the capping layers indicate the presence of unknown carbanious materials which are chemically and structurally different from the oleic acid, oleylamine and/or their complex combinations. FTIR spectra of heat treated samples of $\text{Fe}_{0.4}\text{Co}_{0.6}$, $\text{Fe}_{0.6}\text{Co}_{0.4}$ and $\text{Fe}_{0.8}\text{Co}_{0.2}$ are shown in Figure 1. The FTIR study confirms

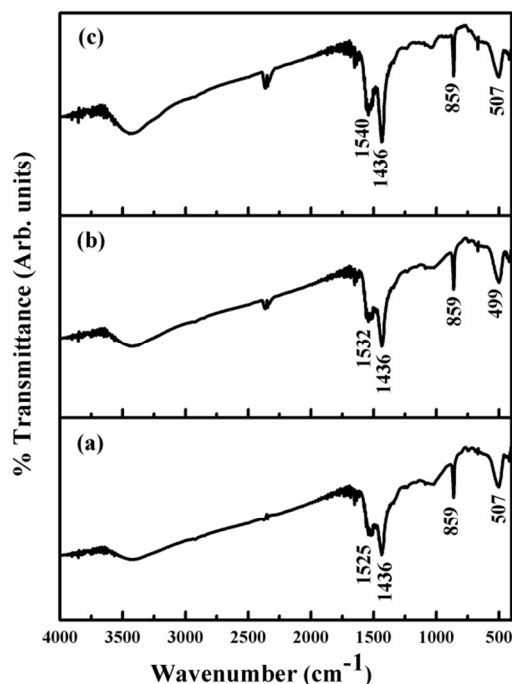


Figure 1. FTIR spectra of (a) $\text{Fe}_{0.4}\text{Co}_{0.6}$, (b) $\text{Fe}_{0.6}\text{Co}_{0.4}$ and (c) $\text{Fe}_{0.8}\text{Co}_{0.2}$ nanomaterials heat treated at 600°C under N_2 atmosphere.

the absence of pure oleic acid and oleylamine at the surface of the nanoparticles. The above mentioned observation is evident from the absence of characteristic peaks at 1708, 2669, 2850-3000, 1654, 1592, and 3325 cm^{-1} .¹⁸ The FTIR spectra of the heat treated FeCo materials indicate strong absorption bands at wavenumbers 1525, 1436, 859, and 507 cm^{-1} . These results are quite similar to our earlier investigations on the nature of capping on the pure Co and Ni nanoparticles¹⁸ irrespective of the alloy compositions. The presence of peaks at 1525 cm^{-1} and 1436 cm^{-1} indicate the presence of some minor fractions of the materials containing carboxylate group (COO^-).¹⁹ The presence of organic capping layer after the heat treatment of the as-prepared oleic acid/oleylamine capped particles is believed to be playing a role in stabilizing from surface oxidation of nanoparticles even at room temperature.

3.2 Solid state reactivity and XRD studies:

$\text{Fe}_x\text{Co}_{1-x}$ ($0.2 \leq x \leq 0.8$) alloys with different compositions were synthesized under similar experimental conditions as mentioned earlier. As synthesized FeCo alloy nanocrystals were amorphous in nature as examined by XRD. The as synthesized alloys were heat treated at various temperatures (400-600 °C) under nitrogen gas atmosphere in order to increase the crystallinity of the materials and to observe any order-disorder phase transformation. However, we have optimized the minimum temperature, i.e. 600 °C, required for the crystallization of FeCo alloys in order to obtain ultrafine particles. XRD patterns of FeCo alloys having different compositions, i.e. $\text{Fe}_x\text{Co}_{1-x}$ ($0.2 \leq x \leq 0.8$), heat treated at 600 °C are shown in Figure 2. We have

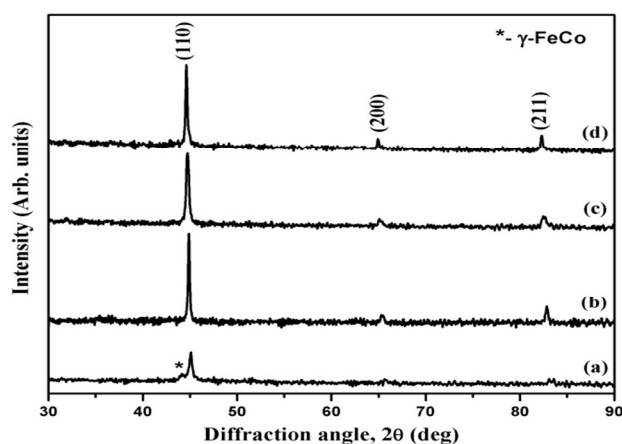


Figure 2. XRD patterns of (a) $\text{Fe}_{0.2}\text{Co}_{0.8}$, (b) $\text{Fe}_{0.4}\text{Co}_{0.6}$, (c) $\text{Fe}_{0.6}\text{Co}_{0.4}$ and (d) $\text{Fe}_{0.8}\text{Co}_{0.2}$ alloys nanoparticles heat treated at 600 °C for 2 h under N_2 atmosphere.

observed that Fe_{0.2}Co_{0.8} alloy contains major bcc (α) and minor fcc (γ) whereas FeCo alloy phases having Fe content(x) above 0.4, show single α -FeCo alloy phase. These results are in accordance with the phase diagram.^{20,21} During the formation of FeCo alloys, it has been observed that Co can diffuse into the α -Fe structure in order to form Fe-Co solid solution.²⁰ Thus, the presence of mixture of α and γ phases simultaneously in Fe_{0.2}Co_{0.8} alloy may be because of large Co content that exceeds the solubility limit (72-90 % of Co content) for the formation of Fe-Co solid solution at room temperature.²¹

TABLE 1: Compositions, crystalline phases, (hkl) values, d values and lattice parameters for FeCo alloys NPs with different compositions.

Composition	Crystalline phase	(hkl) values	d values (Å)		Lattice parameters, a (Å)
			Observed	Calculated	
Fe _{0.2} Co _{0.8}	Bcc	(110)	2.0090	2.0057	2.836(±4)
		(200)	1.4203	1.4182	
		(211)	1.1543	1.1580	
Fe _{0.4} Co _{0.6}	Bcc	(110)	2.0196	2.0173	2.852(±2)
		(200)	1.4254	1.4265	
		(211)	1.1642	1.1647	
Fe _{0.6} Co _{0.4}	Bcc	(110)	2.0225	2.0220	2.859(±1)
		(200)	1.4306	1.4298	
		(211)	1.1665	1.1674	
Fe _{0.8} Co _{0.2}	Bcc	(110)	2.0282	2.0280	2.868(±1)
		(200)	1.4346	1.4340	
		(211)	1.1704	1.1709	

The XRD peaks were broad in nature. This result indicates the signature of nano-crystalline nature of the materials. Spacing between the crystal planes (d-values) and lattice parameters were estimated by least square method and are summarized in Table 1. Crystallite

sizes for FeCo alloys are represented in Table 2. The observed XRD peak positions are indexed in accordance with JCPDS card for α -FeCo alloy (JCPDS # 49-1567) (Figure 2). The compositions (i.e. $\text{Fe}_x\text{Co}_{1-x}$ ($0.4 \leq x \leq 0.8$)) studied in the present work are within the regime where one can expect order-disorder transformation above 400°C . However, the (100) superlattice peak position at 2θ values of $\sim 36.4^\circ$ is not observed in the XRD patterns of the annealed FeCo materials up to a temperature of 600°C .²² Suppression of phase transformation in ultrafine nano-materials is not uncommon in the literature,^{23,24} however, for Fe-Co systems using the present synthetic strategy is the first time report. The shift in the peak positions and increase in the lattice parameters were observed with the increase in Fe content in FeCo alloys. These results confirm the formation of α -FeCo solid solution where Fe atoms are in bcc phase.²⁵ The calculated values of lattice parameters (a) for α - $\text{Fe}_x\text{Co}_{1-x}$ alloys are $2.836(\pm 4)\text{ \AA}$, $2.852(\pm 2)\text{ \AA}$, $2.859(\pm 1)\text{ \AA}$ and $2.868(\pm 1)\text{ \AA}$ for $x = 0.2, 0.4, 0.6$ and 0.8 , respectively. The lattice parameters show increasing trend with progressive increase in Fe content in the materials and are indicative of the fact that alloy formation has taken place.²⁶ The calculated lattice parameters for FeCo alloys are comparable, but slightly less than the value for bulk α -Fe, i.e. 2.866 \AA .²⁷ Average crystallite sizes for the synthesized FeCo alloys were found to be in the range of $\approx 23\text{-}38\text{ nm}$ for the heat treated materials. In summary, synthesis of disordered FeCo alloys at temperatures even up to 600°C in nano-crystalline form has been achieved in the present work.

TABLE 2: Compositions, crystallite sizes, TEM particle sizes, saturation magnetizations (M_s), corrected saturation magnetizations (M'_s), remanent magnetizations (M_r) and coercivity (H_c) values for FeCo alloy NPs with different compositions.

Composition	Crystallite size (nm)	TEM Particle size (nm)	Saturation magnetization, M_s (emu/g)	Saturation magnetization M'_s (emu/g) after correction for CHN content	Remanent Magnetization, M_r (emu/g)	Coercivity, H_c (Oe)
$\text{Fe}_{0.2}\text{Co}_{0.8}$	23.30(± 3)	11.0(± 5)	--	--	--	--
$\text{Fe}_{0.4}\text{Co}_{0.6}$	37.93(± 1)	51.0(± 5)	92.5(± 1)	142.2	2.2	244
$\text{Fe}_{0.6}\text{Co}_{0.4}$	26.06(± 2)	35.0(± 9)	67.1(± 1)	100.1	9.3	400
$\text{Fe}_{0.8}\text{Co}_{0.2}$	38.27(± 2)	24.0(± 2)	71.1(± 0.5)	93.1	10.4	472

3.3 Micro-structural studies:

TEM micrographs for FeCo alloys heat treated at 600 °C are shown in Figure 3. Inset in Figure 3(b) shows typical SAED pattern for $\text{Fe}_{0.4}\text{Co}_{0.6}$. The estimated average particle sizes for FeCo alloys from TEM micrographs are summarized in Table 2. TEM micrograph studies confirm that the synthesized FeCo alloys have nearly spherical morphologies. Average particle sizes for FeCo alloys, estimated from TEM micrographs ranges from 11 nm to 51 nm and are comparable with the average crystallite sizes obtained using XRD technique, i.e. 23 to 38 nm. TEM particle size distributions are reasonably narrow and are evident from the estimated size deviation of 0.4-1.8 nm from average values (Table 2). SAED pattern shows the formation of broader diffraction rings which indicates polycrystalline nature of the materials. The diffraction

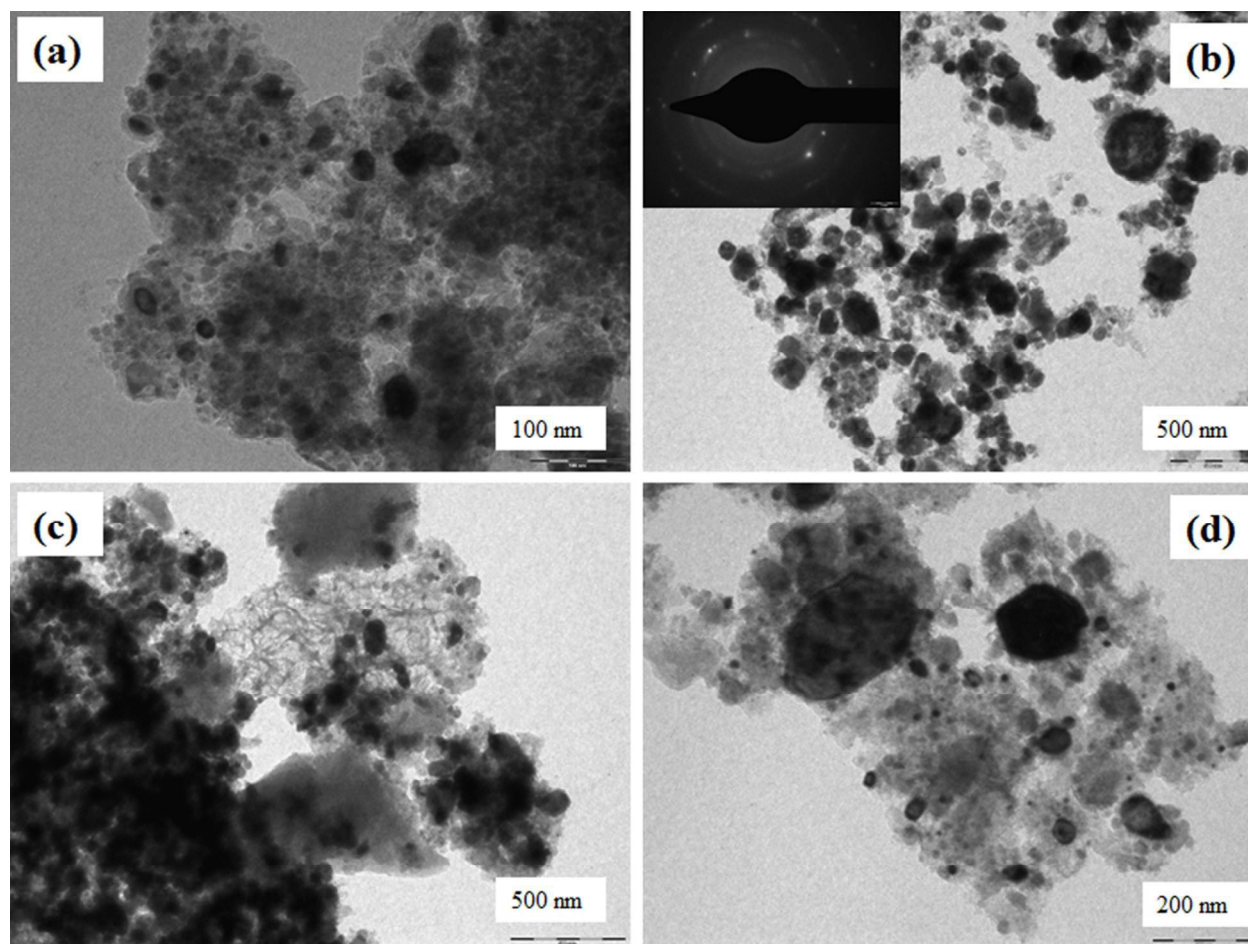


Figure 3. TEM micrographs of (a) $\text{Fe}_{0.2}\text{Co}_{0.8}$, (b) $\text{Fe}_{0.4}\text{Co}_{0.6}$, (c) $\text{Fe}_{0.6}\text{Co}_{0.4}$ and (d) $\text{Fe}_{0.8}\text{Co}_{0.2}$ alloys nanoparticles heat treated at 600 °C for 2 h under N_2 atmosphere. Inset in (b) shows typical SAED pattern for the corresponding alloy.

from the crystalline planes, i.e. (110), (200), (211) etc. in SAED pattern for FeCo alloys for all compositions matches exactly with the XRD results and confirm the formation of α -FeCo alloy phase. In addition, the lattice parameters values obtained from SAED patterns, i.e. $2.79(\pm 1)$, $2.845(\pm 7)$, $2.856(\pm 5)$ and $2.80(\pm 2)$ Å for $\text{Fe}_x\text{Co}_{1-x}$, $x = 0.2, 0.4, 0.6$ and 0.8 , respectively, agrees well with the corresponding values obtained from XRD results (Table 1).

3.4 Magnetic studies:

Room temperature magnetic hysteresis loops (M vs H curves) for $\text{Fe}_x\text{Co}_{1-x}$ alloys ($x = 0.4, 0.6, 0.8$) have been shown in Figure 4 and the inset represents the corresponding values of the M_s . Thermo-magnetic measurements have also been carried out in order to investigate temperature dependent magnetic properties of the alloys. As $\text{Fe}_{0.2}\text{Co}_{0.8}$ alloy crystallizes with mixture of two phases, i.e. fcc and bcc, the material is excluded while investigating the composition dependent of magnetization. The as synthesized materials obtained at 600°C ; contain organic coating at the surface. Therefore, two different values of M_s are reported herewith, i.e. one denotes M_s without considering wt% of organic layer and the other, M'_s , after wt % corrections corresponding to CHN content. Considering the very high values of C/H ratios, the oxygen content is assumed to be negligibly small and not considered while estimating the

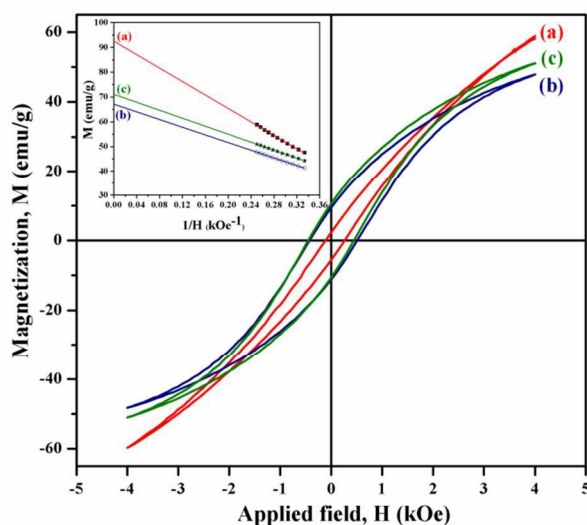


Figure 4. Room temperature magnetic hysteresis loops for (a) $\text{Fe}_{0.4}\text{Co}_{0.6}$, (b) $\text{Fe}_{0.6}\text{Co}_{0.4}$ and (c) $\text{Fe}_{0.8}\text{Co}_{0.2}$ alloys nanoparticles heat treated at 600°C for 2 h under N_2 atmosphere. Inset represents corresponding the M Vs $1/H$ plots for determining the values of saturation magnetization.

corrected values for M_s . Variation in both the values of M_s and M'_s (as obtained and after corrections) and coercivity (H_c) with various Fe content (x) in the FeCo alloys have been shown in Figure 5 (a, b and c). Temperature dependence of the magnetization plots in FC and ZFC conditions at 100 Oe of applied field are presented in Figure 6. The values of the M_s of the materials were determined by M vs $1/H$ law which was employed for the bulk materials and M_s was obtained by the intercepts on magnetization axis.²⁸ It is to be noted that in fine particle systems, M vs H plots do not get saturated and the increase in magnetizations are achieved by spin rotation only. The estimated extrapolated values of the M_s , remanent magnetization (M_r) and coercivities (H_c) for FeCo alloys are tabulated in Table 2. The values of M_s , M_r and H_c for Fe_xCo_{1-x} alloys ($x = 0.4, 0.6, 0.8$) are found to be in the range of 71.1-92.5 emu/g, 2.2-10.4 emu/g and 244-472 Oe, respectively. After corrections employed for wt% of organic coatings, the values of the M_s are estimated in the range of 93.1-142.2 emu/g for Fe_xCo_{1-x} alloys ($x = 0.4, 0.6, 0.8$).

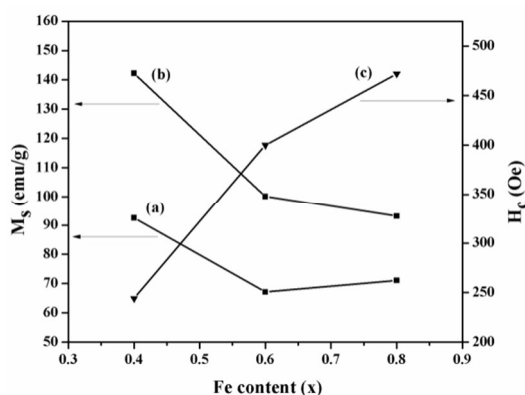


Figure 5. Plot of variations in values of saturation magnetization, M_s , for (a) without wt% corrections for organic content, (b) after correction (M'_s), and (c) coercivity, H_c , with respect to Fe content in the Fe_xCo_{1-x} alloys ($x = 0.4, 0.6, 0.8$).

The magnetic hysteresis loops confirm that FeCo alloys exhibit ferromagnetic behavior at room temperature (Figure 4). The values of M_s , i.e. 71.1-92.5 emu/g, and 93.1-142.2 emu/g, for FeCo alloys having organic coating and after correction for wt% for organic coating are smaller than the values reported for bulk ordered materials (i.e. 245 emu/g).²⁹ This may be attributed to the combined effects of altered crystal anisotropies, disordered structure, reduction in particle size and spin canting at the surface of nanomaterials.³⁰ It has been established by Zeng et al.²⁹ that reduction of M_s (say maximum up to ≈ 15 emu/g) is observed as a result of disordering in the

distribution of Fe and Co atoms in the crystal structure. The disordered structure has already been established by our XRD results. Although, almost constancy in magnetic anisotropy may be observed at least up to room temperature for ideal FeCo bulk magnetic materials, significant alteration may not be over ruled for nano materials. Therefore, additional reduction in magnetization at room temperature may be attributed to thermal effects at our measurement temperature, i.e. 298K. The estimated maximum value of M_s , i.e. 143 emu/g, for $Fe_{0.4}Co_{0.6}$ alloy composition after correction for organic capping, is still significantly lower than the bulk saturation, i.e. 245 emu/g. This result indicates the signature of onset of fine particle size and surface effects including superparamagnetism in FeCo alloys synthesized by the present strategy and such reduction has already observed in several magnetic materials.^{23,31}

With the reduction of particle dimension, size and surface effects becomes predominant in nanomaterials. The size effects include the origin of superparamagnetism as a result of thermal randomization of the magnetic moments. The surface effects majorly originate from canted spin structure of the magnetic materials.^{23,31} It should be noted that specific magnetization vs field plots of FeCo alloys at room temperature do not saturate upto an applied field of 4000 Oe. These results confirm the presence of superparamagnetic fractions in the alloy materials. Also, it is observed that there is alteration of M_s values with Fe content in the Fe_xCo_{1-x} alloys (figure 5). It should be noted that magnetic saturation is related to positions and arrangements of atoms in the crystal structure and resultant magnetization may be dependent on magnetic exchange interactions among atomic moments.³² Also, it is reported that M_s values for FeCo alloys are composition dependent and may vary with concentration of Fe in the Fe_xCo_{1-x} ($0.4 \leq x \leq 0.8$) nanomaterials.³³ With the increase in Fe at% (x) in FeCo alloys, the values of M_s , initially increases, shows a maximum ($\approx x=0.5$) and thereafter decreases. The shifting of the maximum is dependent on materials structure obtained by using alternative synthetic methods.^{33, 34} In our study, we obtained gradual decrease in the values of M_s with increase in the Fe at% (x) (from x = 0.4 to 0.8) measured at room temperature from M vs H plots and after applying the corrections for CHN content (Figure 5(b)). Although, particle size distribution and presence of superparamagnetic fractions may influence the values of M_s , in the present study, effect of composition of the FeCo alloys is dominant for the decreasing trend of the M_s values. It should be noted that the wt% correction abruptly increases the values of M'_s compared to M_s with the

increase of Co content. The abrupt changes may result from the small variation of organic content due to different chemical affinity of nano-materials with different composition, even though the synthetic parameters are similar.

The variation of H_c of Fe_xCo_{1-x} ($0.4 \leq x \leq 0.8$) nanomaterials with gradual increase in the values of x has been shown in Figure 5(c) and the values of M_r are presented in Table 2. The gradual increase in the values of H_c with increasing Fe content may be attributed to different size and surface morphologies along with composition.^{34,35} It has been reported in the literature that H_c values are inversely proportional to the grain size of the material above a critical size and our results are in accordance with the literature reports.²⁹ The reduced values of the ratios of remanent magnetization and saturation magnetization, i.e. M_r/M_s , of the Fe_xCo_{1-x} alloys are found to be 0.02, 0.13 and 0.14 for x equal to 0.4, 0.6 and 0.8, respectively. This indicates that crystal anisotropies increase with the increase in Fe content and supports the increasing trend in the values of the coercivities. Such kinds of results have already been reported in the literature for FeCo system.³⁶

FC and ZFC magnetization measurements of Fe_xCo_{1-x} alloys ($x = 0.4, 0.6, 0.8$) (Figure 6) show similar behavior with magnetic irreversibility below room temperature (i.e. 300 K). Magnetization in the FC curves include contribution from all particles whereas ZFC curves consider magnetization from such nanoparticles whose energy barriers are overcome by thermal energy ($k_B T$) at that temperature.³⁷ The FC magnetization values are higher than the ZFC magnetization values and indicate the presence of ferromagnetism in our samples up to at least 300 K. In all FeCo alloys, the ZFC magnetization increases rapidly with temperature and is not superimposed with FC curve up to 300 K which indicates that the nanoparticles are in the magnetically blocked state. This blocking of nanoparticles may be attributed to stronger dipolar interparticle magnetic interactions.³⁵ Strength of such a dipolar interactions increases with increase in particle magnetic moments and decrease in distance between them. In the present study, the observed higher values of coercivities (244-474 Oe) indicate strong dipolar interactions amongst the particles. This is evident from the literature reported results that FeCo bulk materials are expected to show reduced coercivities ($\sim 10-60$ Oe)³⁵ and with a reduction of particle sizes to a value of 10-60 nm range, moderate increase in the values of H_c (102 Oe) is

observed.³⁸ Hence deviations in the FC/ZFC curves are mainly related to dipolar interactions in adjacent particles. At temperatures greater than 300 K, we can expect superimposition of FC/ZFC curves and hence superparamagnetic behavior of the materials. Assuming the spherical nature of the nanoparticles, the K_{eff} can be calculated by using the formula, $K = 25k_B T_B/V$, where T_B is blocking temperature, V is particle volume and k_B is the Boltzmann constant.³⁹ Assuming the value of blocking temperature (T_B) equal to 300 K and the particle volume from TEM, the K_{eff} of $\text{Fe}_x\text{Co}_{1-x}$ alloys were calculated to be 1.5 kJ/m^3 , 4.6 kJ/m^3 and 14.3 kJ/m^3 for the values of x equal to 0.4, 0.6 and 0.8, respectively. To be noted, Penget al. determined the magnetic anisotropy energy (40 kJ/m^3) for $\text{Fe}_{0.7}\text{Co}_{0.3}$ nanoparticles.⁴⁰ These values are comparable but relatively lower than the respective values of FeCo alloys with small Co content.⁴¹ Similarly Bansmann et al.⁴² obtained a magnetic anisotropy energy of $K = 190\text{--}200 \text{ kJ/m}^3$ for 10 nm FeCo nanoparticles. However, we observed reduction in magnetic anisotropy energy in our FeCo compositions compared to the literature reported values for 10 nm FeCo alloys. This may be attributed to alteration of size of the nanoparticles and surface anisotropy

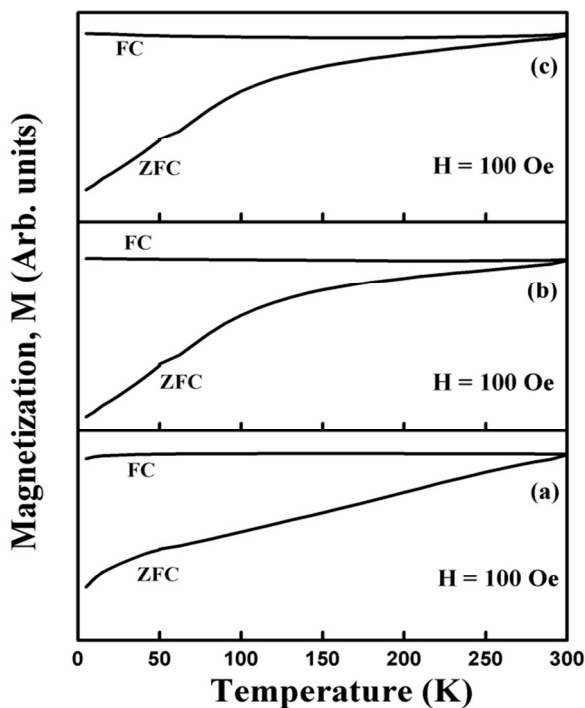


Figure 6. Temperature dependence of magnetization curves for (a) $\text{Fe}_{0.4}\text{Co}_{0.6}$, (b) $\text{Fe}_{0.6}\text{Co}_{0.4}$ and (c) $\text{Fe}_{0.8}\text{Co}_{0.2}$ alloys in field cooled (FC) and zero field cooled (ZFC) conditions. The applied field employed is 100 Oe.

contribution.³⁹ Further investigations are needed on the origin and quantification of surface magnetic anisotropy in FeCo alloys.

3.5 Mössbauer Spectroscopic studies:

The room temperature Mössbauer spectra of $\text{Fe}_x\text{Co}_{1-x}$ alloys ($x = 0.4, 0.6, 0.8$) have been shown in Figure 7 along with its fitted sub-spectra for clarity reason. The values of hyperfine field (H_{hf}), isomer shift (δ), line width and relative intensities of the fitted sub spectra are

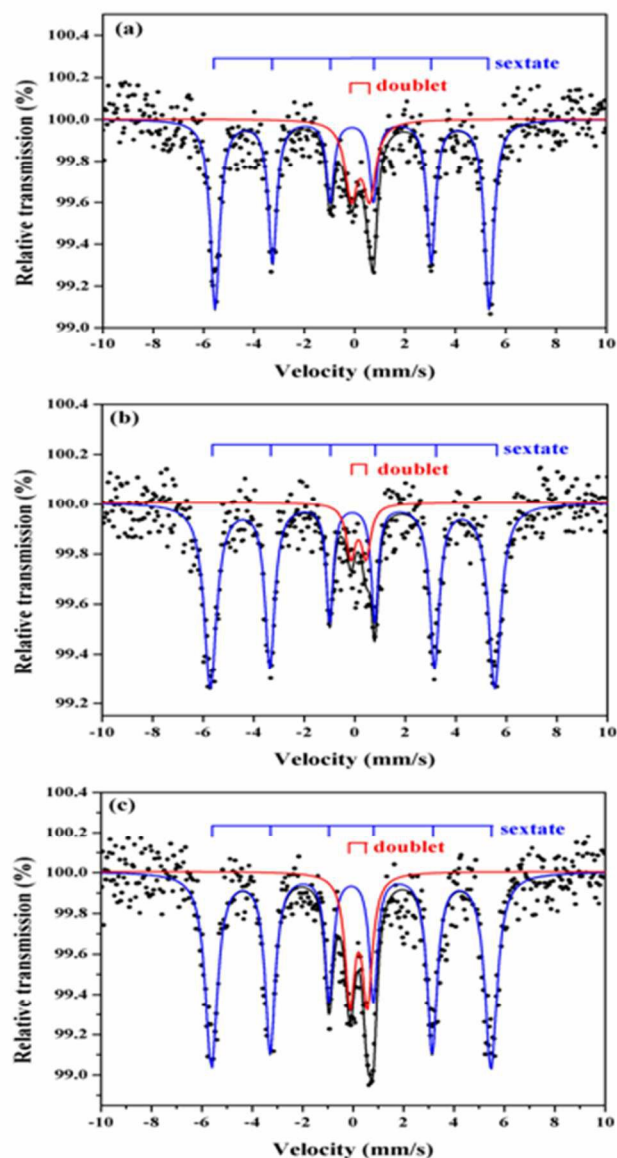


Figure 7. Room temperature Mössbauer spectra of (a) $\text{Fe}_{0.4}\text{Co}_{0.6}$, (b) $\text{Fe}_{0.6}\text{Co}_{0.4}$ and (c) $\text{Fe}_{0.8}\text{Co}_{0.2}$ alloy nanoparticles.

summarized in Table 3. The Mössbauer spectrum of $\text{Fe}_{0.2}\text{Co}_{0.8}$ did not show well defined Mössbauer absorption. This may be attributed to the presence of less amount of Fe content and mixture of two phases in the structure of the alloy. The Mössbauer spectra of $\text{Fe}_{0.4}\text{Co}_{0.6}$, $\text{Fe}_{0.6}\text{Co}_{0.4}$ and $\text{Fe}_{0.8}\text{Co}_{0.2}$ having crystallite sizes of 38 nm, 26 nm and 38 nm, respectively, were deconvoluted into ferromagnetic sextet and superparamagnetic doublet of FeCo material. The relative intensity of the sextet:doublet in $\text{Fe}_{0.4}\text{Co}_{0.6}$, $\text{Fe}_{0.6}\text{Co}_{0.4}$ and $\text{Fe}_{0.8}\text{Co}_{0.2}$ alloys are 80:20, 90:10 and 80:20, respectively. As the relative intensity of the doublet and sextet is related to the fraction of superparamagnetic nanoparticles present in the materials, saturation magnetizations in the alloys may differ significantly. This indicates the fine particle nature of our materials with particle size distribution. The presence of one sextet indicates single Fe site with equivalent chemical environment in FeCo alloys. Interpretation of Mössbauer data of FeCo alloys with one sextet has already been reported for materials synthesized by sonochemical method.⁴³ The line widths of the Mössbauer spectra are broaden, i.e. 0.44 mm/s, 0.52 mm/s and 0.54 mm/s. This may be attributed to the random substitution of Fe atoms by Co ones with hyperfine field distributions. It has been reported in the literature that Mössbauer spectra of $\text{Fe}_{50}\text{Co}_{50}$ powders are characterized by broadened line-width with a shoulder of the outmost lines.^{44,45} However, in the Mössbauer spectra, we did not observe such shoulder in the outmost lines which indicates pure phase nature of the materials.

TABLE 3: The values of hyperfine fields (H_{hf}), isomer shifts (δ), line widths and relative intensities for fitted sub spectra of FeCo alloys with different compositions.

Composition	Sub Spectrum	Mössbauer Parameters			
		H_{hf} (T)	Isomer Shift, δ (mm/s)	Line widths, (mm/s)	Relative Intensity (%)
$\text{Fe}_{0.4}\text{Co}_{0.6}$	Sextet	33.8	0.005	0.44	80
	Doublet	---	0.342	0.60	20
$\text{Fe}_{0.6}\text{Co}_{0.4}$	Sextet	34.9	0.017	0.52	90
	Doublet	---	0.255	0.45	10
$\text{Fe}_{0.8}\text{Co}_{0.2}$	Sextet	34.4	0.033	0.54	80
	Doublet	---	0.329	0.45	20

The values of the H_{hf} for sextet (i.e. 33.8 T, 34.9 T and 34.4 T for $Fe_{0.4}Co_{0.6}$, $Fe_{0.6}Co_{0.4}$ and $Fe_{0.8}Co_{0.2}$, respectively) are higher than that of pure α -Fe ($H_{hf} = 33.3$ T)⁴⁶ and comparable with the literature reported values i.e. 33.8 T, 35.4 T and 36.4 T for $Fe_{0.4}Co_{0.6}$, $Fe_{0.6}Co_{0.4}$ and $Fe_{0.8}Co_{0.2}$, respectively.⁴⁷ This confirms the formation of pure FeCo alloys. In the materials under study, we have obtained variation in H_{hf} values with respect to composition of FeCo alloy with maximum value for $Fe_{0.6}Co_{0.4}$ alloy. These variations may be attributed to the change in magnetic environment at the Fe nucleus in FeCo alloys with composition. Further, the discrepancies in H_{hf} values may be attributed to the disordered magnetic structures at the surface of nanomaterials. These kinds of surface effects on the hyperfine field have been reported in literature.⁴⁸ Kodama et al. have already been reported that the H_{hf} value equal to 36 T for $Fe_{48}Co_{52}$ alloy nanoparticles which is greater than the value for ordered $Fe_{50}Co_{50}$ alloy (i.e. 35 T).³³ However, H_{hf} values, i.e. 33.8-34.9 T, for the FeCo alloys in the present study are in the range where one can expect disordered FeCo alloys characteristics.⁴⁹ One can expect increase in magnetic moment of Fe atom with increase of Fe content in the FeCo alloys. However, referring to magnetic study, we do not observe such trend in the values of M_s . This is attributed to presence of reduced size, surface effects and superparamagnetic fractions in the materials. Thus, the Mössbauer study appropriately corroborates the magnetic characteristics.

The Mössbauer parameter, isomer shift (δ) is related to chemical bonding associated with Fe in a solid.⁴⁸ The values of δ for sextet sub-spectra were found to be 0.005 mm/s, 0.017 mm/s and 0.033 mm/s for $Fe_{0.4}Co_{0.6}$, $Fe_{0.6}Co_{0.4}$ and $Fe_{0.8}Co_{0.2}$, respectively. These values of δ are smaller but comparable to the value reported for disordered $Fe_{50}Co_{50}$ alloy (i.e. 0.035 mm/s).⁵⁰ The values of δ for doublet sub-spectra were found to be 0.342 mm/s, 0.255 mm/s and 0.329 mm/s for $Fe_{0.4}Co_{0.6}$, $Fe_{0.6}Co_{0.4}$ and $Fe_{0.8}Co_{0.2}$, respectively. Although, δ values indicate Fe to be in higher oxidation state, we do not observe Fe-oxide phase in our XRD and Mössbauer investigation. Thus, the doublet spectrum is attributed to the presence of superparamagnetic fractions present in the materials.

4 Conclusions

In summary, FeCo alloy nanoparticles of various compositions have been synthesized via superhydride reduction route with altered magnetic properties. FTIR study indicates organic coatings at the surface of the particles which helps in stabilizing the FeCo alloy nanoparticles in air atmosphere. XRD patterns confirm that the $\text{Fe}_x\text{Co}_{1-x}$ alloys ($x = 0.4, 0.6, 0.8$) crystallize in pure α -FeCo alloy phase and the values of lattice parameters increases with Fe content. The crystallite sizes were found to be in the range of ≈ 23 -38 nm. TEM micrograph studies prove nearly spherical morphologies with narrow particle size distribution of the synthesized FeCo alloys. Average particle sizes estimated from TEM micrographs range from 11 nm to 51 nm. The values of the M_s for FeCo alloys range from 93.1-142.2 emu/g after corrections for organic wt % at the surface of the materials. These values are quite large for Fe-Co materials while considering the small size nature of the materials and may be useful for potential technological applications. Variation of saturation magnetization with compositions was interpreted on the basis of varied compositions, reduction in particle size, altered crystal anisotropies and spin canting at the surface of nanomaterials. Low temperature FC/ZFC magnetization measurements show magnetic irreversibility and blocking of nanoparticles due to strong dipolar interparticle magnetic interactions. Estimated values of K_{eff} of $\text{Fe}_x\text{Co}_{1-x}$ alloys (i.e. 1.5 kJ/m³, 4.6 kJ/m³ and 14.3 kJ/m³ for $x = 0.4, 0.6$ and 0.8, respectively) reveal the contribution from the reduced particle size and surface anisotropy. Room temperature Mössbauer studies show presence of ferromagnetic sextet and superparamagnetic doublet in FeCo materials. The variations in the values of H_{hf} in FeCo alloys may be attributed to the change in magnetic structure at the Fe nucleus with composition and disordered magnetic structures at the surface of the nanoparticles. Thus, a structure-property correlation in FeCo alloys has been attempted in this investigation.

Acknowledgment

For this investigation, we gratefully acknowledge the financial support from Council of Scientific and Industrial Research (CSIR), New Delhi and Department of Science and Technology (DST), New Delhi. We acknowledge SAIF, IIT Bombay, Mumbai for TEM measurements. We also express our thanks to Prof. K. P. Rajeev, IIT Kanpur for SQUID magnetic measurements.

References

- 1 G. S. Chaubey, C. Barcena, N. Poudyal, C. Rong, J. Gao, S. Sun and J. P. Liu, *J. Am. Chem. Soc.*, 2007, **129**, 7214.
- 2 C. Jo, J. Lee and Y. Jang, *Chem. Mater.*, 2005, **17**, 2667.
- 3 H. Zeng, J. Li, J. P. Liu, Z. L. Wang and S. Sun, *Nature*, 2002, **420**, 395.
- 4 W. S. Seo, J. H. Lee, X. Sun, Y. Suzuki, D. Mann, Z. Liu, M. Terashima, P. C. Yang, M. V. Mcconnell and D. G. Nishimura, *Nat. Mater.*, 2006, **5**, 971.
- 5 N. Takano, N. Hosoda, T. Yamada and T. Osaka, *J. Electrochem. Soc.*, 1999, **146**, 1407.
- 6 S. Behrens, H. Bonnemann, N. Matoussevitch, A. Gorschinski, E. Dinjus, W. Habicht, J. Bolle, S. Zinoveva, N. Palina, J. Hormes, H. Modrow, S. Bahr and V. Kempter, *J. Phys.: Condens. Matter.*, 2006, **18**, S2543.
- 7 X. G. Liu, D. Y. Geng and Z. D. Zhang, *Appl. Phys. Lett.*, 2008, **92**, 243110.
- 8 X. Gao, S. C. Tan, A. T. S. Wee, J. Wu, L. Kong, X. Yu and H. O. Moser, *J. Electron Spectrosc. Relat. Phenom.*, 2006, **150**, 11.
- 9 V. Tzitzios, G. Basina, D. Niarchos, L. Wangfeng and G. Hadjipanayis, *J. Appl. Phys.*, 2011, **109**, 07A313.
- 10 S. K. Pal and D. Bahadur, *Mater. Lett.*, 2010, **64**, 1127.
- 11 D. Hisada, Y. Fujiwara, H. Sato, M. Jimbo, T. Kobayashi and K. Hata, *J. Magn. Mater.*, 2011, **323**, 3184.
- 12 M. Zamanpour, Y. Chen, B. Hu, K. Carroll, Z. J. Huba, E. E. Carpenter, L. H. Lewis and V. G. Harris, *J. Appl. Phys.*, 2012, **111**, 07B528.
- 13 A. Corrias, M. F. Casula, A. Falqui and G. Paschina, *Chem. Mater.*, 2004, **16**, 3130.
- 14 S. S. Parhizgar and S. A. Sebt, *J. Theor. Appl. Phys.*, 2013, **7**, 44.

- 15 M. Hesani, A. Yazdani, B. AbediRavan and M. Ghazanfari, *Solid State Commun.*, 2010, **150**, 594.
- 16 C. M. Shen, C. Hui, T. Z. Yang, C. W. Xiao, S. T. Chen, H. Ding and H. J. Gao, *Chin. Phys. Lett.*, 2008, **25**, 1479.
- 17 B. D. Cullity, *Elements of X-ray diffraction*, Reading MA: Addison Wesley, 1956, pp. 98.
- 18 S. B. Dalavi and R. N. Panda, *J. Magn. Magn. Mater.*, 2015, **374**, 411.
- 19 W. Kemp, *Organic Spectroscopy*, Palgrave, N. Y., 3rd Edn., 1991, pp. 30.
- 20 A. Zelenakova, D. Oleksakova, J. Degmova, J. Kovac, P. Kollar, M. Kusy and P. Sovak, *J. Magn. Magn. Mater.*, 2007, **316**, e519.
- 21 T. Soumail, *Prog. Mater. Sci.*, 2005, **50**, 816.
- 22 G. B. Chon, K. Shinoda, S. Suzuki and B. Jeyadevan, *Mater. Trans.*, 2010, **51**, 707.
- 23 R.N. Panda and N. S. Gajbhiye, *J. Appl. Phys.*, 1999, **86**, 3295.
- 24 H. H. Hsiao, R. N. Panda, J. C. Shih and T. S. Chin, *J. Appl. Phys.*, 2002, **91**, 3145.
- 25 P. Karipoth, A. Thirumuruganand R. Justin Joseyphus, *J. Colloid Interface Sci.*, 2013, **404**, 49.
- 26 M. Kaur, Q. Dai, M. Bowden, M. Engelhard, Y. Wu, J. Tang and Y. Qiang, *Appl. Phys. Lett.*, 2013, **103**, 202407.
- 27 R. S. Sundar and S. C. Deevi, *Int. Mater. Rev.*, 2005, **50**, 157.
- 28 C. P. Bean and I. S. Jacobs, *J. Appl. Phys.*, 1960, **31**, 1228.
- 29 Q. Zeng, I. Baker, V. McCreary and Z. Yan, *J. Magn. Magn. Mater.*, 2007, **318**, 28.
- 30 M. Kaur, J. S. McCloy, W. Jiang, Q. Yao and Y. Qiang, *J. Phys. Chem. C*, 2012, **116**, 12875.
- 31 S. Morup, E. Brok and C. Frandsen, *J. Nano Mat.*, 2013, **2013**, Article ID 720629.
- 32 A. Azizi, S. K. Sadmezhaad and A. Hasani, *J. Magn. Magn. Mater.*, 2010, **322**, 3551.

- 33 D. Kodama, K. Shinoda, K. Sato, Y. Konno, R. J. Joseyphus, K. Motomiya, H. Takahashi, T. Matsumoto, Y. Sato, K. Tohji and B. Jeyadevan, *Adv. Mater.*, 2006, **18**, 3154.
- 34 G. H. Lee, S. H. Huh, J. W. Jeong, S. H. Kim, B. J. Choi, J. H. Jeong, H. I. Lee and H. C. Ri, *J. Korean Phys. Soc.*, 2003, **42**, 367.
- 35 X. W. Wei, G. X. Zhu, Y. J. Liu, Y. H. Ni, Y. Song and Z. Xu, *Chem. Mater.*, 2008, **20**, 6248.
- 36 D. Ung, G. Viau, C. Ricolleau, F. Warmont, P. Gredin and F. Fieffer, *Adv. Mater.*, 2005, **17**, 338.
- 37 J. Kim, J. Kim, J. Kim and K. H. Kim, *J. Appl. Phys.*, 2013, **113**, 17A313.
- 38 S. Alikhanzadeh-Arani, M. Salavati-Niasari and M. Almasi-Kashi, *J. Magn. Magn. Mater.*, 2012, **324**, 3652.
- 39 E. M. M. Ibrahim, S. Hampel, A. U. B. Wolter, M. Kath, A. A. El-Gendy, R. Klingeler, C. Taschner, V. O. Khavrus, T. Gemming, A. Leonhardt and B. Buchner, *J. Phys. Chem. C*, 2012, **116**, 2209.
- 40 D. L. Peng, Y. Chena, H. Shea, R. Katoh and K. Sumiyama, *J. Alloys Compd.*, 2009, **469**, 276.
- 41 R. C. Hall, *J. Appl. Phys.*, 1960, **31**, 1037.
- 42 J. Bansmann, A. Kleibert, M. Getzlaff, A. F. Rodriguez, F. Nolting, C. Boeglin and K. H. Meiwes-Broer, *Phys. Status Solidi B*, 2010, **247**, 1152.
- 43 Q. Li, H. Li, V. G. Pol, I. Bruckental, Y. Koltypin, J. Calderon-Moreno, I. Nowik and A. Gedanken, *New J. Chem.*, 2003, **27**, 1194.
- 44 H. Moumeni, S. Alleg and J. M. Greneche, *J. Alloys Compd.*, 2005, **386**, 12.
- 45 J. Zarpellon, H. F. Jurca, N. Mattoso, J. J. Klein, W. H. Schreiner, J. D. Ardisson, W. A. A. Macedo and D. H. Mosca, *J. Colloid Interface Sci.*, 2007, **316**, 510.
- 46 M. F. Casula, G. Concas, F. Congiu, A. Corrias, A. Falqui and G. Spano, *J. Phys. Chem. B*, 2005, **109**, 23888.

- 47 C. E. Johnson, M. S. Ridout and T. E. Cranshaw, *Proc. Phys. Soc.*, 1963, **81**, 1079.
- 48 R. N. Panda and N. S. Gajbhiye, *J. Appl. Phys.*, 1997, **81**, 335.
- 49 J. E. Frackowiak, *Hyperfine Interact.*, 1990, **60**, 757.
- 50 H. H. Hamdeh, B. Fultz and D. H. Pearson, *Phys. Rev. B*, 1989, **39**, 11233.

TABLE 1: Compositions, crystalline phases, (hkl) values, d values and lattice parameters for FeCo alloys NPs with different compositions.

Composition	Crystalline phase	(hkl) values	d values (Å)		Lattice parameters, a (Å)
			Observed	Calculated	
Fe _{0.2} Co _{0.8}	Bcc	(110)	2.0090	2.0057	2.836(±4)
		(200)	1.4203	1.4182	
		(211)	1.1543	1.1580	
Fe _{0.4} Co _{0.6}	Bcc	(110)	2.0196	2.0173	2.852(±2)
		(200)	1.4254	1.4265	
		(211)	1.1642	1.1647	
Fe _{0.6} Co _{0.4}	Bcc	(110)	2.0225	2.0220	2.859(±1)
		(200)	1.4306	1.4298	
		(211)	1.1665	1.1674	
Fe _{0.8} Co _{0.2}	Bcc	(110)	2.0282	2.0280	2.868(±1)
		(200)	1.4346	1.4340	
		(211)	1.1704	1.1709	

TABLE 2: Compositions, crystallite sizes, TEM particle sizes, saturation magnetizations(M_s), corrected saturation magnetizations(M'_s), remanent magnetizations(M_r) and coercivity(H_c) values for FeCo alloy NPs with different compositions.

Composition	Crystallite size (nm)	TEM Particle size (nm)	Saturation magnetization, M_s (emu/g)	Saturation magnetization M'_s (emu/g) after correction for CHN content	Remanent Magnetization, M_r (emu/g)	Coercivity, H_c (Oe)
Fe _{0.2} Co _{0.8}	23.30(±3)	11.0(±5)	--	--	--	--
Fe _{0.4} Co _{0.6}	37.93(±1)	51.0(±5)	92.5(±1)	142.2	2.2	244
Fe _{0.6} Co _{0.4}	26.06(±2)	35.0(±9)	67.1(±1)	100.1	9.3	400
Fe _{0.8} Co _{0.2}	38.27(±2)	24.0(±2)	71.1(±0.5)	93.1	10.4	472

TABLE 3: The values of hyperfine fields (H_{hf}), isomer shifts(δ), line widths and relative intensities for fitted sub spectra of FeCo alloys with different compositions.

Composition	Sub Spectrum	Mössbauer Parameters			
		H_{hf} (T)	Isomer Shift, δ (mm/s)	Line widths, (mm/s)	Relative Intensity (%)
$Fe_{0.4}Co_{0.6}$	Sextet	33.8	0.005	0.44	80
	Doublet	---	0.342	0.60	20
$Fe_{0.6}Co_{0.4}$	Sextet	34.9	0.017	0.52	90
	Doublet	---	0.255	0.45	10
$Fe_{0.8}Co_{0.2}$	Sextet	34.4	0.033	0.54	80
	Doublet	---	0.329	0.45	20

CAPTIONS FOR FIGURES

Figure 1. FTIR spectra of (a) $\text{Fe}_{0.4}\text{Co}_{0.6}$, (b) $\text{Fe}_{0.6}\text{Co}_{0.4}$ and (c) $\text{Fe}_{0.8}\text{Co}_{0.2}$ nanomaterials heat treated at 600 °C under N_2 atmosphere.

Figure 2. XRD patterns of (a) $\text{Fe}_{0.2}\text{Co}_{0.8}$, (b) $\text{Fe}_{0.4}\text{Co}_{0.6}$, (c) $\text{Fe}_{0.6}\text{Co}_{0.4}$ and (d) $\text{Fe}_{0.8}\text{Co}_{0.2}$ alloys nanoparticles heat treated at 600 °C for 2 h under N_2 atmosphere.

Figure 3. TEM micrographs of (a) $\text{Fe}_{0.2}\text{Co}_{0.8}$, (b) $\text{Fe}_{0.4}\text{Co}_{0.6}$, (c) $\text{Fe}_{0.6}\text{Co}_{0.4}$ and (d) $\text{Fe}_{0.8}\text{Co}_{0.2}$ alloys nanoparticles heat treated at 600 °C for 2 h under N_2 atmosphere. Inset in (b) shows typical SAED pattern for the corresponding alloy.

Figure 4. Room temperature magnetic hysteresis loops for (a) $\text{Fe}_{0.4}\text{Co}_{0.6}$, (b) $\text{Fe}_{0.6}\text{Co}_{0.4}$ and (c) $\text{Fe}_{0.8}\text{Co}_{0.2}$ alloys nanoparticles heat treated at 600 °C for 2 h under N_2 atmosphere. Inset represents corresponding the M vs $1/H$ plots for determining the values of saturation magnetization.

Figure 5.Plot of variations in values of saturation magnetization, M_s , for (a) without wt% corrections for organic content, (b) after correction (M'_s), and (c) coercivity, H_c , with respect to Fe content in the $\text{Fe}_x\text{Co}_{1-x}$ alloys ($x = 0.4, 0.6, 0.8$).

Figure 6. Temperature dependence of magnetization curves for (a) $\text{Fe}_{0.4}\text{Co}_{0.6}$, (b) $\text{Fe}_{0.6}\text{Co}_{0.4}$ and (c) $\text{Fe}_{0.8}\text{Co}_{0.2}$ alloys in field cooled (FC) and zero field cooled (ZFC) conditions. The applied field employed is 100 Oe.

Figure 7.Room temperature Mössbauer spectra of (a) $\text{Fe}_{0.4}\text{Co}_{0.6}$, (b) $\text{Fe}_{0.6}\text{Co}_{0.4}$ and (c) $\text{Fe}_{0.8}\text{Co}_{0.2}$ alloy nanoparticles.

Observation of strong dipolar interactions leading to improved magnetic properties of chemically synthesized $\text{Fe}_x\text{Co}_{1-x}$ alloy nano-materials (size range, 24-51 nm).

